Enhancing Airflow and Thermal Performance in Narrow-Body Aircraft Cabins: A CFD-RSM Approach Applied to the Airbus A320

Emmanuel Udama Odeh[1]

Department of Mechanical and Aerospace Engineering

University of Uyo, Uyo, Akwa Ibom State, Nigeria

emmanuelodeh@uniuyo.edu.ng

Emenike Peculiar Akachukwu[2]

Department of Mechanical and Aerospace Engineering

University of Uyo, Uyo, Akwa Ibom State, Nigeria

emenikepeculiar@gmail.com

Abstract

This study evaluates airflow and thermal performance in an Airbus A320 economy-class cabin section using computational fluid dynamics (CFD) and Response Surface Methodology (RSM). A three-dimensional transverse cabin-section model was developed in ANSYS DesignModeler and discretised with tetrahedral meshes. The simulations were solved in ANSYS Fluent using a pressure-based steady RANS formulation, the realizable k-ε turbulence model and the energy equation. A 24-run parametric design varied inlet velocity, inlet temperature, seat pitch and mesh refinement. Average cabin velocity was used as a bulk airflow response, while maximum cabin air temperature was used as a conservative thermal response. The simulated average cabin velocity ranged from 0.10 to 0.27 m/s, and the maximum cabin temperature ranged from 22.7 to 28.0 °C. Inlet velocity dominated the airflow response, while inlet temperature dominated the thermal response. Seat pitch also affected both responses because it changed local passage geometry around the seat row. The fitted RSM models gave high agreement within the investigated design space, with reported R^2 values of 0.9991 for average cabin velocity and 0.9995 for maximum cabin temperature. Multi-response desirability optimisation predicted an inlet velocity of 0.201 m/s, inlet temperature of 20.595 °C, seat pitch of 0.709 m and mesh refinement of 150,000 cells. The corresponding predicted responses were 0.099 m/s average cabin velocity and 24.275 °C maximum cabin temperature, with a composite desirability of 1.000. The result identifies a low-draught, thermally acceptable operating region that should be verified by a confirmatory CFD case before design use.

Keywords: Airbus A320 cabin; computational fluid dynamics; environmental control system; airflow distribution; thermal performance; Response Surface Methodology; desirability optimisation.

1. Introduction

Aircraft environmental control systems (ECS) supply fresh and recirculated conditioned air into a confined cabin where passengers, seats, sidewalls and supply jets interact over short distances. The engineering challenge is not only to meet air-exchange and pressurisation requirements, but also to move heat and momentum in a way that limits draught, stagnant pockets and local temperature peaks. Thermal comfort theory shows that passengers respond to the local combination of air temperature, air speed, turbulence and radiant exchange rather than to cabin-average conditions alone [1-3].

The Airbus A320 provides a practical case for this problem because it is a widely used single-aisle aircraft with a dense economy-class layout and a mixing-ventilation arrangement. Conditioned air introduced near the upper cabin region must pass around seats, passengers and sidewall curvature before leaving through lower outlet paths. This geometry promotes jet deflection, recirculation and local differences between aisle, middle and window-seat regions. Previous cabin-ventilation studies have shown that such features can produce uneven airflow distribution, local thermal discomfort and contaminant-retention zones even where overall ventilation rates are high [4-7].

CFD is useful for this class of problem because it can resolve velocity and temperature fields before expensive full-scale testing is attempted. It also permits parametric changes in inlet velocity, supply temperature, seat pitch and mesh resolution under a common numerical framework. Nevertheless, CFD results are only useful when the geometry, boundary conditions, mesh quality, turbulence closure and model limitations are stated clearly. The realizable k-ε model remains widely used for repeated internal-flow simulations because it gives a practical balance between numerical stability and computational cost, although higher-fidelity turbulence models may be needed for transient or occupant-resolved studies [8-10].

Response Surface Methodology helps convert a finite CFD campaign into an interpretable design model. It identifies dominant factor effects, shows interactions and supports multi-response optimisation where airflow and thermal objectives compete. Desirability optimisation is appropriate here because high supply momentum may improve flushing but may also increase draught risk, while colder supply air reduces temperature peaks but may not guarantee local comfort [11-13].

This study assesses airflow and thermal performance together in an Airbus A320 economy-class cabin section. Average cabin velocity is used as a bulk airflow response, and maximum cabin temperature is used as a conservative thermal response. The analysis identifies an ECS operating region for later verification with local comfort and velocity-distribution metrics.

2. Materials and methods

2.1 Research design and workflow

The study followed a coupled CFD-RSM workflow. The airflow and thermal responses were extracted from the same converged CFD cases, fitted separately and then combined at the desirability-optimisation stage. This structure was used because the factors that improve thermal response are not always the same as those that influence the bulk airflow field.

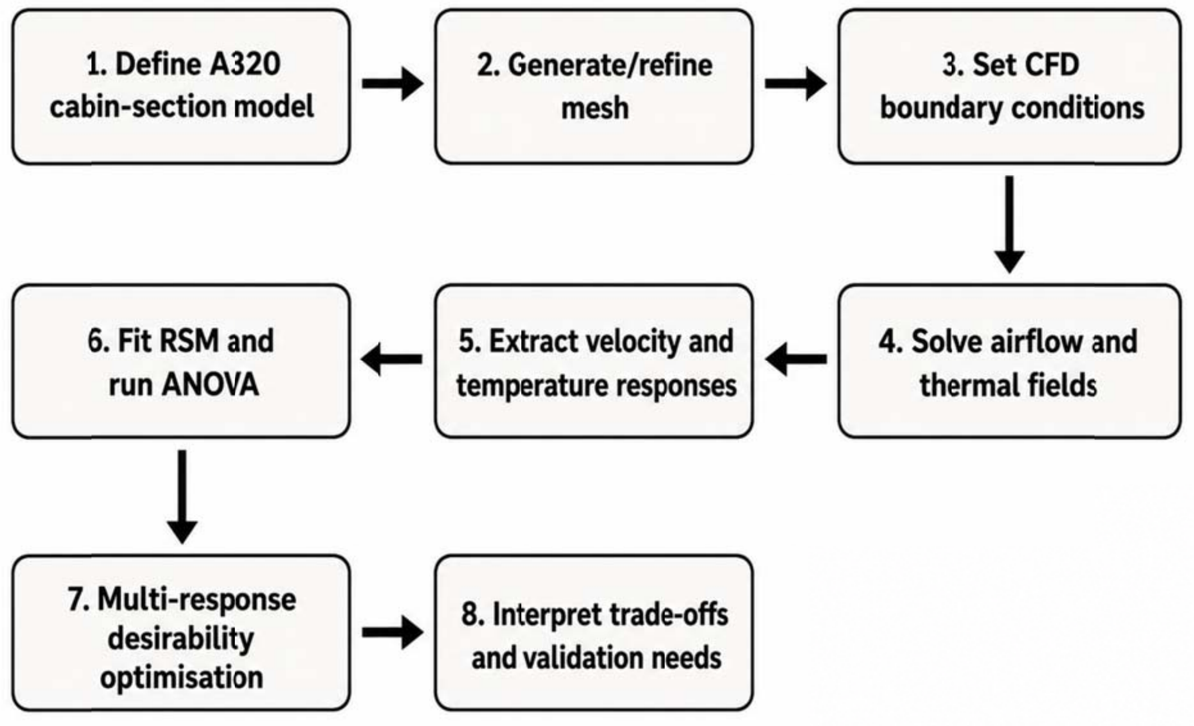

Figure 1. CFD-RSM workflow used for the coupled airflow and thermal-performance assessment.

2.2 Cabin geometry and modelling assumptions

The computational domain represented a three-dimensional transverse economy-class section of the Airbus A320 cabin. The geometry retained the curved cabin envelope, seat-row blockage, main supply-air regions and outlet paths. Small fittings that do not control the main airflow were omitted so that the simulation campaign could remain repeatable. The simplification preserved the features most relevant to jet deflection, passage restriction, recirculation and heat removal.

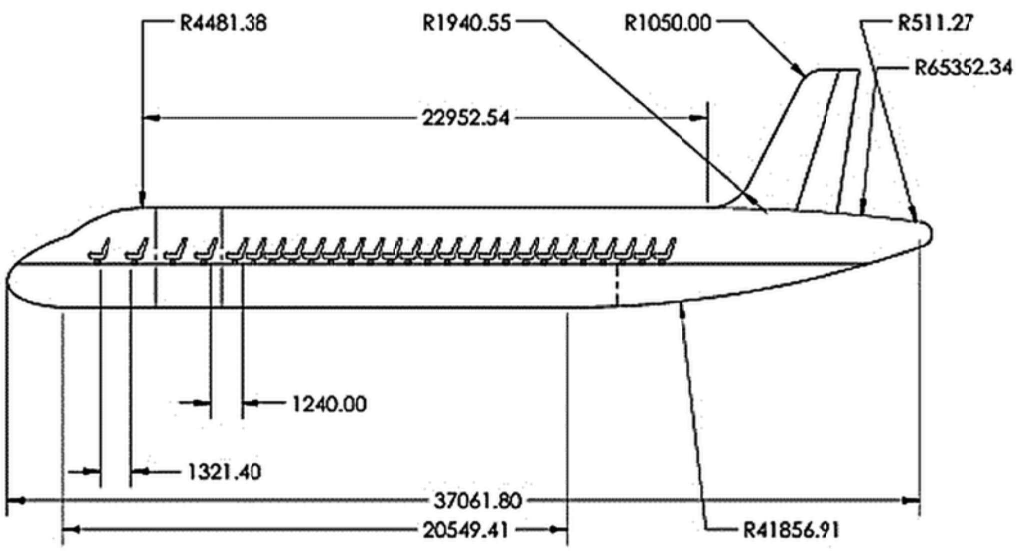

Figure 2. A320 cabin geometry reference used to guide the computational model.

The cabin airflow was treated as low-Mach-number internal flow. Air was modelled as a Newtonian fluid with constant thermophysical properties for the parametric comparison, while thermal coupling was resolved through the energy equation. The inlet boundary used the prescribed velocity and temperature from the design matrix, walls and seats were no-slip surfaces, and the outlet was treated as a pressure outlet. Seat pitch was varied as a cabin-layout factor because the row spacing changes the passages through which the supplied air moves after entry.

2.3 Mesh generation and quality control

The cabin section was discretised using an unstructured tetrahedral mesh. Refinement was concentrated near the inlet region, outlets, seat surfaces and wall-adjacent zones where strong velocity and temperature gradients were expected. Mesh refinement was included as a numerical-control factor rather than as an ECS operating variable. This allowed the fitted model to distinguish physical ECS effects from numerical sensitivity.

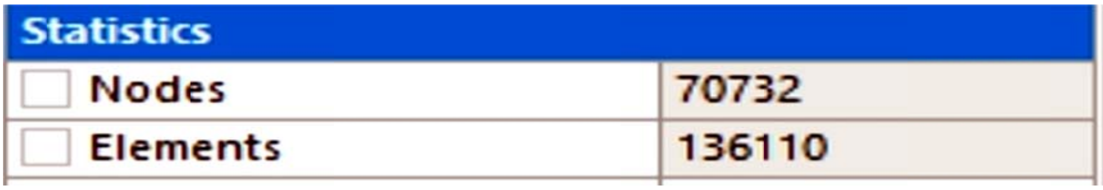

Statistics	
Nodes	70732
Elements	136110

Figure 3. Screenshot of the Mesh-statistics output from the ANSYS meshing stage.

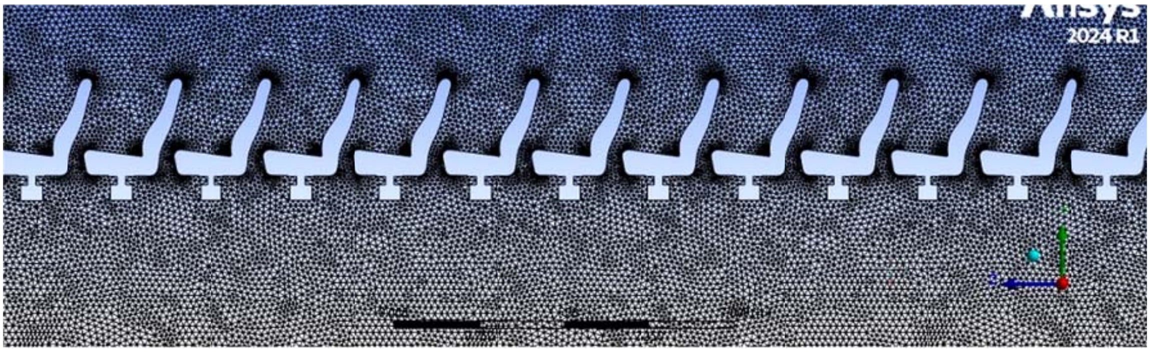

Figure 4. Tetrahedral mesh used for the A320 cabin CFD model.

Mesh quality was evaluated using skewness and orthogonal-quality indicators. The mesh-quality checks were necessary because poor element quality can create false recirculation, unstable residual histories or artificial temperature peaks. The final response extraction used the same post-processing procedure for all cases, so that differences between runs reflected the imposed factor settings rather than inconsistent evaluation methods.

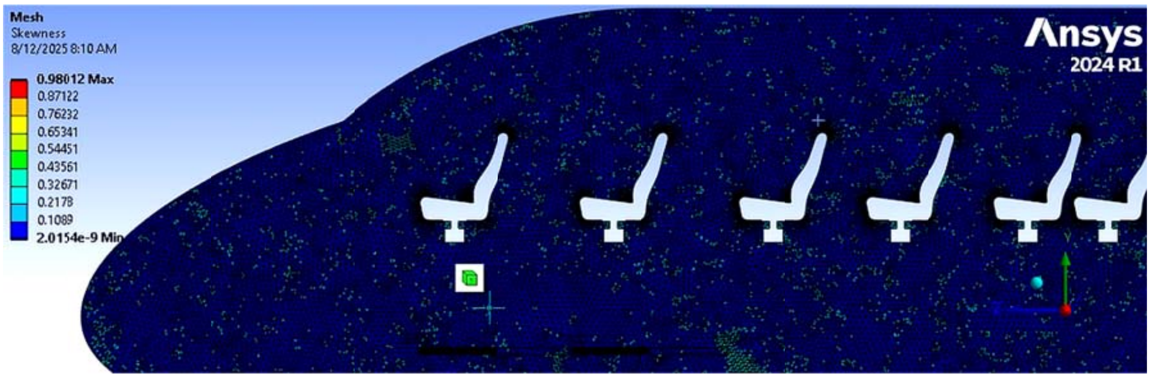

Figure 5. Skewness distribution from the ANSYS mesh-quality check.

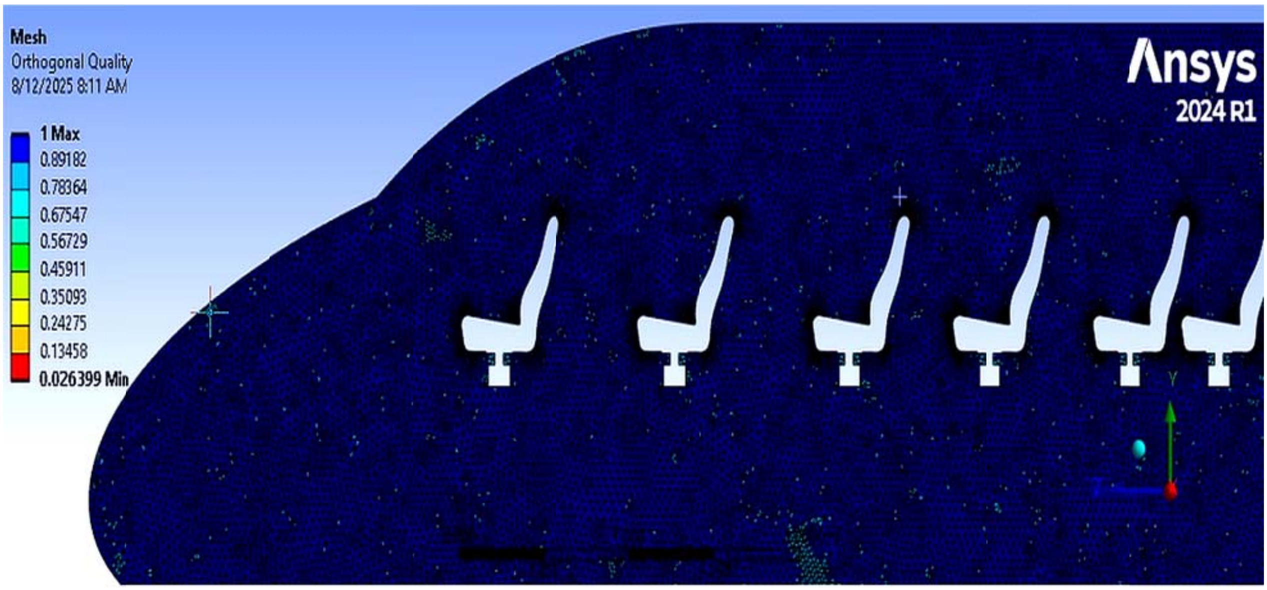

Figure 6. Orthogonal-quality distribution from the ANSYS mesh-quality check.

2.4 Solver settings and boundary conditions

The CFD simulations were solved using a pressure-based finite-volume formulation suitable for low-speed cabin airflow. A steady RANS approach was used for the parametric assessment, with the realizable k-ε turbulence model selected for stable prediction of mixed indoor and cabin jets. The energy equation was activated to resolve the thermal field. Pressure-velocity coupling and second-order transport discretisation were applied where stable convergence was obtained. Residual reduction was checked together with monitored stabilisation of the average cabin velocity and maximum cabin temperature. The solver setup followed the ANSYS Fluent pressure-based formulation [14], and the realizable k-ε closure followed the model of Shih et al. [15].

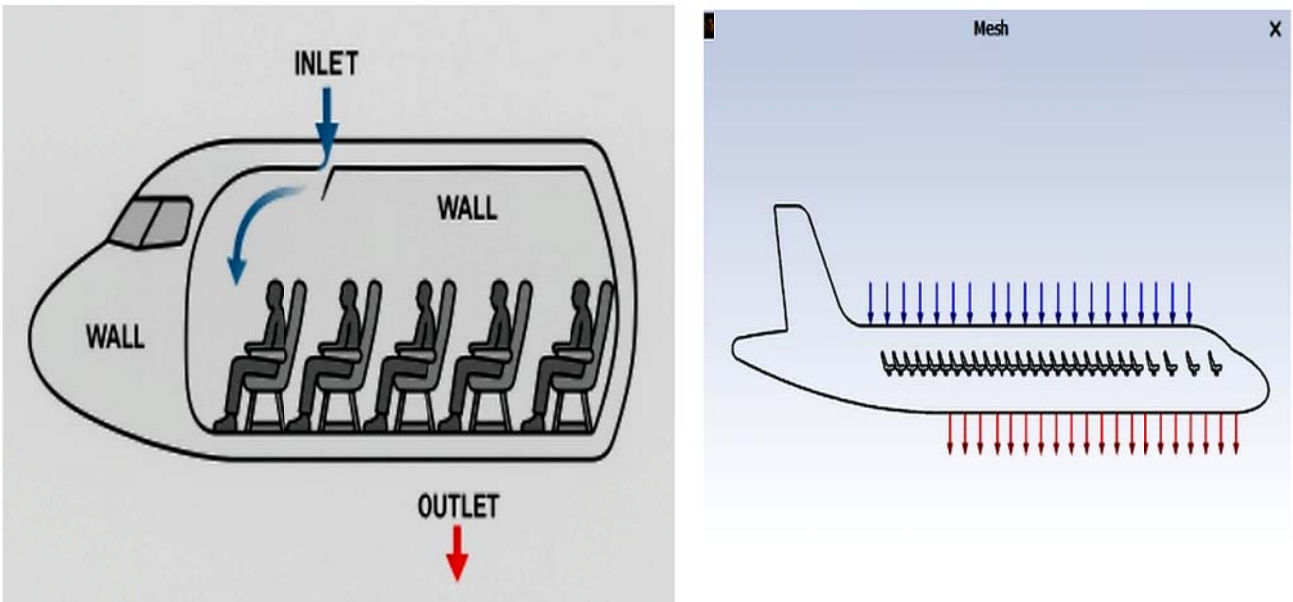

Figure 7. Boundary-condition screenshots for the A320 cabin-section CFD model.

Table 1. CFD solver and boundary-condition settings.

Item	Setting used in the CFD campaign	Role in the simulation

Item	Setting used in the CFD campaign	Role in the simulation
Solver type	Pressure-based finite-volume solver	Low-speed internal cabin airflow
Flow model	Steady RANS	Parametric assessment of ECS settings
Turbulence closure	Realizable k-ε model	Practical closure for repeated cabin-jet simulations
Energy model	Energy equation activated	Prediction of thermal gradients and maximum temperature
Computational space	Three-dimensional transverse cabin section	Consistent with the tetrahedral-mesh cabin model
Inlet boundary	Velocity inlet, 0.20-0.60 m/s	Physical ECS supply-momentum factor
Inlet temperature	20.0-25.0 °C	Supply-air thermal factor
Outlet boundary	Pressure outlet	Exhaust path from the cabin section
Wall and seat surfaces	Stationary no-slip walls	Representation of cabin envelope and seat blockage
Mesh levels	100,000-150,000 cells	Numerical-control factor
Response extraction	Volume-averaged cabin velocity and maximum cabin air temperature	Airflow and thermal responses for RSM fitting

2.5 Governing equations and response-surface formulation

The numerical model solved the conservation equations for mass, momentum and energy. For the low-Mach-number cabin condition, the incompressible continuity equation was written as:

$$\nabla \cdot \mathbf{u} = 0 \quad (1)$$

The steady incompressible momentum equation was expressed as:

$$\rho(\mathbf{u} \cdot \nabla)\mathbf{u} = -\nabla p + \mu \nabla^2 \mathbf{u} + \mathbf{F} \quad (2)$$

The steady energy equation used to resolve the thermal field was expressed as:

$$\rho C_p(\mathbf{u} \cdot \nabla T) = k \nabla^2 T + Q \quad (3)$$

In these equations, u is the velocity vector, p is pressure, T is temperature, ρ is air density, μ is dynamic viscosity, C_p is specific heat capacity, k is thermal conductivity, Q is volumetric heat input and F represents body-force effects. The second-order response-surface model used for each CFD response was written as:

$$Y = \beta_0 + \sum \beta_i x_i + \sum \beta_{ii} x_i^2 + \sum\sum \beta_{ij} x_i x_j + \varepsilon \quad (4)$$

For the combined optimisation, individual desirability values were aggregated using the weighted geometric mean:

$$D = \left(\prod_{i=1}^{n} d_i^{w_i} \right)^{1/\sum_{i=1}^{n} w_i} \quad (5)$$

In Equations (4) and (5), x_i are coded design factors, β terms are regression coefficients, ε is the residual error, d_i is the individual desirability for response i, and w_i is the corresponding response weight.

2.6 Parametric design and response extraction

The parametric design examined four factors: inlet velocity, inlet temperature, seat pitch and mesh-refinement level. In this paper, seat pitch means the row-to-row spacing used in the cabin-section model. The two responses were average cabin velocity and maximum cabin temperature. Average cabin velocity was used as a bulk airflow response, not as a complete spatial uniformity metric. Maximum cabin temperature was used as a conservative thermal response because it identifies the most severe hot region in the evaluated cabin section. Repeated factor combinations in the 24-run matrix were retained as design repetitions for checking residual scatter and model stability within the tested range.

Table 2. CFD-RSM factors and investigated levels.

Code	Factor	Investigated range	Role in the analysis
A	Inlet velocity	0.20-0.60 m/s	Physical ECS supply-momentum factor
B	Inlet temperature	20.0-25.0 °C	Supply-air thermal factor
C	Seat pitch	0.70-0.90 m	Cabin-layout obstruction factor
D	Mesh refinement	100,000-150,000 cells	Numerical-control factor

Table 3. CFD-RSM design matrix and response outcomes used for model fitting.

Run	A: Inlet velocity (m/s)	B: Inlet temperature (°C)	C: Seat pitch (m)	D: Mesh level (cells)	Average cabin velocity (m/s)	Maximum cabin temperature (°C)
1	0.60	22.5	0.90	120,000	0.26	25.2
2	0.60	25.0	0.70	120,000	0.25	27.8
3	0.40	25.0	0.80	120,000	0.18	27.4
4	0.20	20.0	0.70	100,000	0.11	23.7
5	0.40	22.5	0.90	100,000	0.17	24.9
6	0.40	22.5	0.70	100,000	0.16	25.4
7	0.60	22.5	0.80	150,000	0.26	25.3
8	0.40	22.5	0.90	100,000	0.17	24.9
9	0.60	20.0	0.80	100,000	0.27	22.8
10	0.60	20.0	0.90	150,000	0.27	22.7
11	0.40	25.0	0.80	120,000	0.18	27.4
12	0.20	22.5	0.70	120,000	0.10	25.9
13	0.20	20.0	0.80	150,000	0.11	23.1
14	0.20	25.0	0.80	100,000	0.10	27.9
15	0.20	25.0	0.90	150,000	0.11	27.7
16	0.20	25.0	0.90	120,000	0.11	27.7
17	0.20	20.0	0.70	120,000	0.10	23.7
18	0.40	25.0	0.70	150,000	0.17	28.0
19	0.20	25.0	0.80	150,000	0.10	27.9
20	0.60	20.0	0.70	120,000	0.25	23.7
21	0.40	25.0	0.70	120,000	0.17	28.0
22	0.20	20.0	0.80	120,000	0.11	23.1
23	0.40	22.5	0.70	100,000	0.16	25.4
24	0.60	25.0	0.90	100,000	0.25	27.1

3. Results

3.1 Response ranges from the CFD simulation matrix

The 24 CFD runs produced average cabin velocities from 0.10 to 0.27 m/s and maximum cabin temperatures from 22.7 to 28.0 °C. The airflow response increased mainly with inlet velocity, while the maximum-temperature response increased mainly with inlet temperature. Seat pitch changed both responses because the row spacing altered the local passage area available for supply-air mixing.

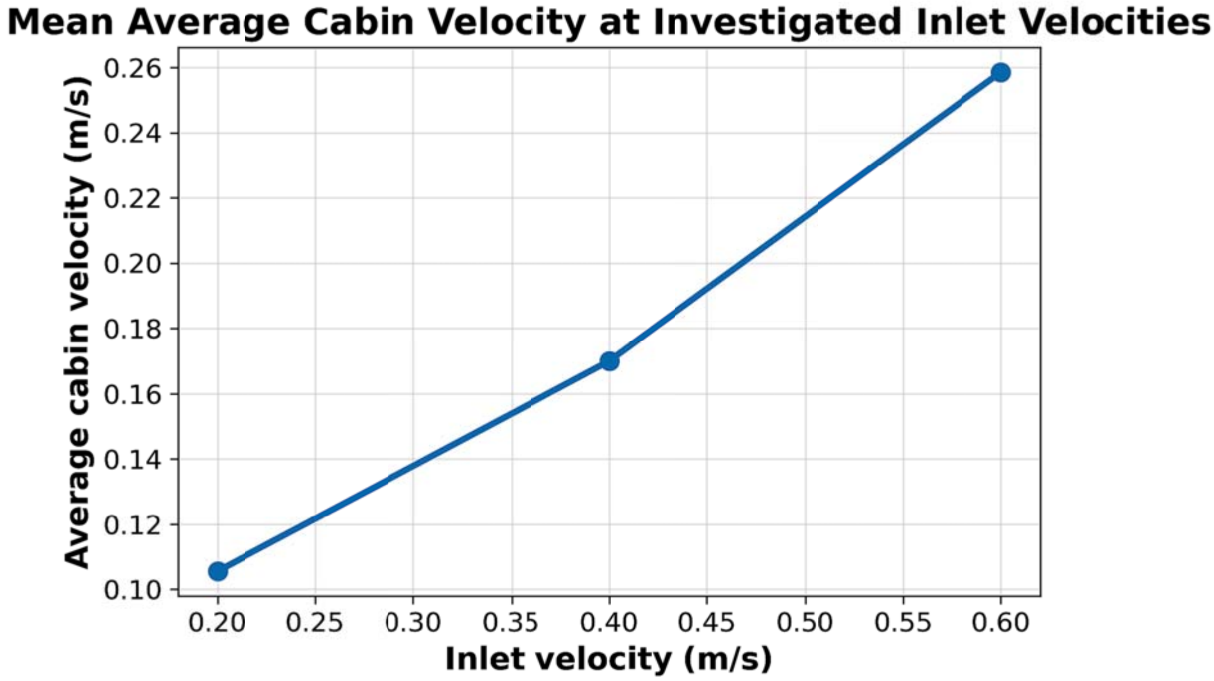

Figure 8. Mean average-cabin-velocity response at the investigated inlet-velocity levels.

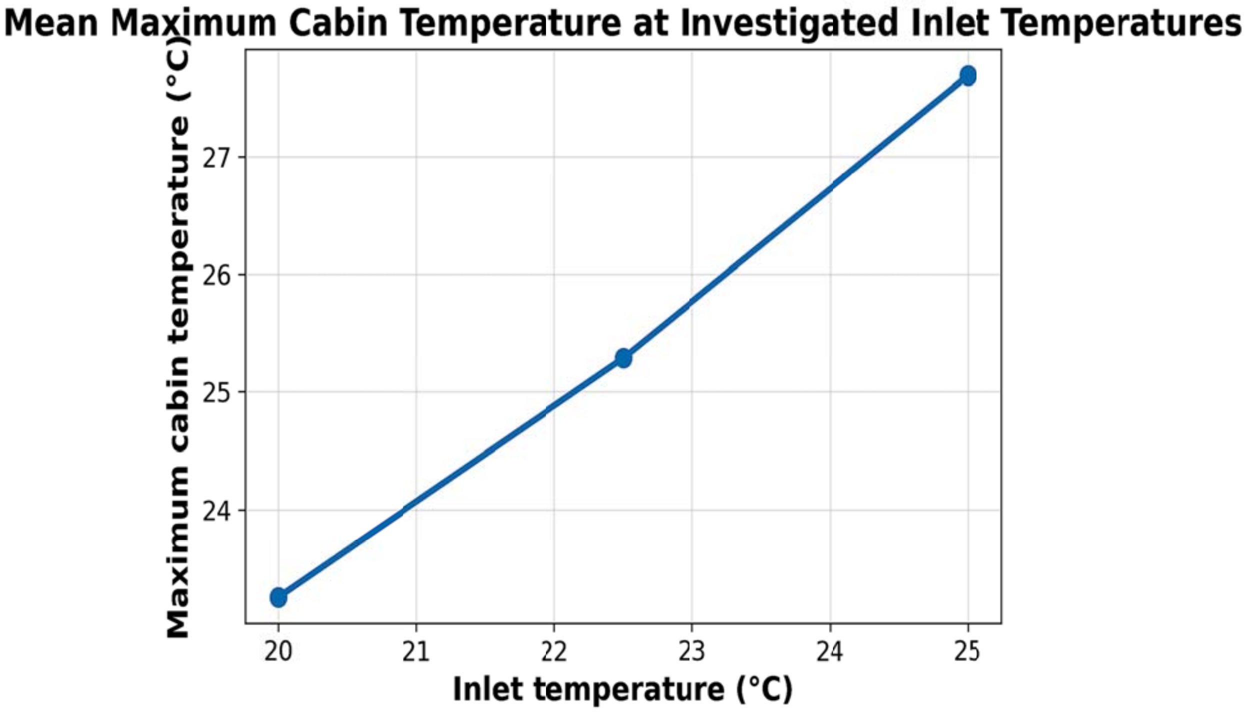

Figure 9. Mean maximum-cabin-temperature response at the investigated inlet-temperature levels.

3.2 Coded-factor coefficient estimates

Table 4. Selected coded-factor coefficient estimates for average cabin velocity.

Term	Coefficient estimate	Interpretation
Intercept	0.176	Mean response at the design centre
A: inlet velocity	0.078	Dominant positive influence on average velocity

Term	Coefficient estimate	Interpretation
B: inlet temperature	-0.001	Weak thermal cross-effect on velocity
C: seat pitch	0.005	Wider spacing increases local passage flow
D_1: mesh level	-0.001	Small numerical-control effect
D_2: mesh level	0.001	Small numerical-control effect

Note: Table 4 lists the dominant and interpretable coded terms. D_1 and D_2 are coded indicator terms representing mesh-refinement levels in the fitted categorical mesh factor.

Only dominant and interpretable coefficients are reported in the coefficient table; the full fitted model retained the terms used in the ANOVA summary. For the average cabin velocity model, inlet velocity had the largest positive coefficient. Seat pitch also had a positive coefficient, indicating that wider row spacing reduced local blockage and allowed stronger average motion in the evaluated cabin section. Mesh-refinement terms were small, which suggests that the bulk velocity response was not strongly controlled by mesh level within the tested range.

Table 5. Selected coded-factor coefficient estimates for maximum cabin temperature.

Term	Coefficient estimate	Interpretation
Intercept	25.42	Mean response at the design centre
A: inlet velocity	-0.26	Higher supply momentum reduces maximum temperature
B: inlet temperature	2.37	Dominant positive thermal influence
C: seat pitch	-0.21	Wider spacing reduces local thermal build-up
D_1: mesh level	0.09	Numerical sensitivity at one mesh level
D_2: mesh level	-0.07	Numerical sensitivity at another mesh level

Note: Table 5 lists selected terms used to interpret the fitted response. D_1 and D_2 are coded indicator terms for mesh-refinement levels.

Only dominant and interpretable coefficients are reported in the coefficient table; the full fitted model retained the terms used in the ANOVA summary. For maximum cabin temperature, inlet temperature had the strongest positive coefficient. Inlet velocity and seat pitch had negative coefficients, suggesting that increased supply momentum and less obstructed passage geometry helped reduce local thermal accumulation.

3.3 ANOVA and model adequacy

Table 6. ANOVA summary for the average cabin velocity response.

Source	Sum of squares	df	Mean square	F-value	p-value	Remark
Model	0.0932	17	0.0055	391.40	<0.0001	Significant
A: inlet velocity	0.0717	1	0.0717	5122.59	<0.0001	Dominant
B: inlet temperature	0.0001	1	0.0001	4.76	0.0718	Weak
C: seat pitch	0.0003	1	0.0003	21.52	0.0035	Significant
D: mesh refinement	0.0001	2	0.0000	2.28	0.1831	Not dominant
Residual	0.0001	6	0.0000	-	-	Error

Table 7. ANOVA summary for the maximum cabin temperature response.

Source	Sum of squares	df	Mean square	F-value	p-value	Remark
Model	74.34	17	4.37	509.72	<0.0001	Significant
A: inlet velocity	0.58	1	0.58	67.63	0.0002	Significant
B: inlet temperature	78.76	1	78.76	9175.02	<0.0001	Dominant
C: seat pitch	0.49	1	0.49	56.89	0.0003	Significant
D: mesh refinement	0.37	2	0.18	21.33	0.0019	Significant numerical effect
Residual	0.05	6	0.01	-	-	Error

The ANOVA results show that the two responses were governed by different dominant factors. The average-velocity model was controlled mainly by inlet velocity, whereas the maximum-temperature model was controlled mainly by inlet temperature. Seat pitch was significant in both models because it changed the obstruction pattern surrounding the seat row. Source sums of squares are model-term or partial sums and are not required to add directly to the model sum of squares.

The fitted response surfaces followed the CFD trends within the 24-run design matrix, with reported R^2 values of 0.9991 for average cabin velocity and 0.9995 for maximum cabin temperature. Because the model retained several terms relative to the number of runs, these R^2 values are treated as within-matrix fit indicators rather than independent predictive validation. The response surfaces are therefore interpreted inside the investigated design space.

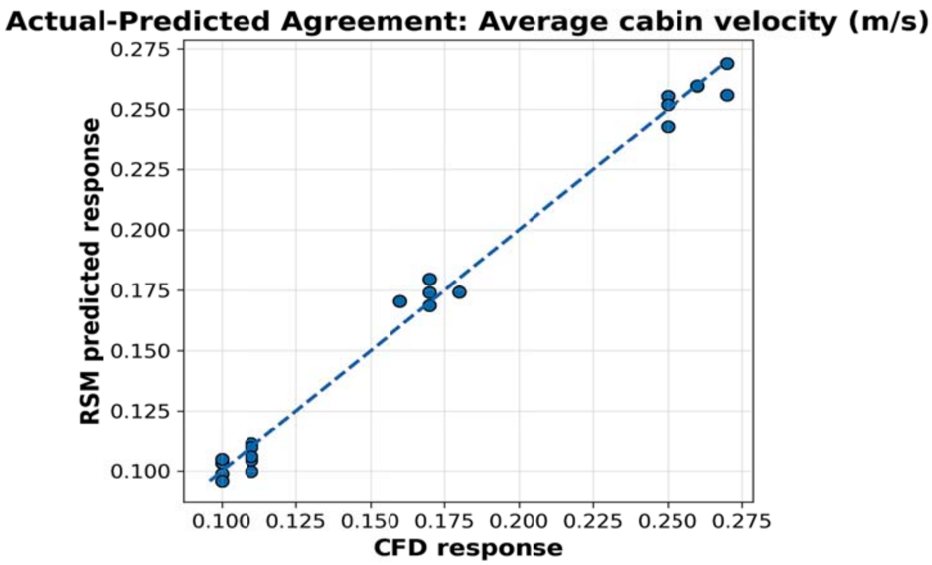

Figure 10. Actual-predicted agreement for the average cabin velocity model.

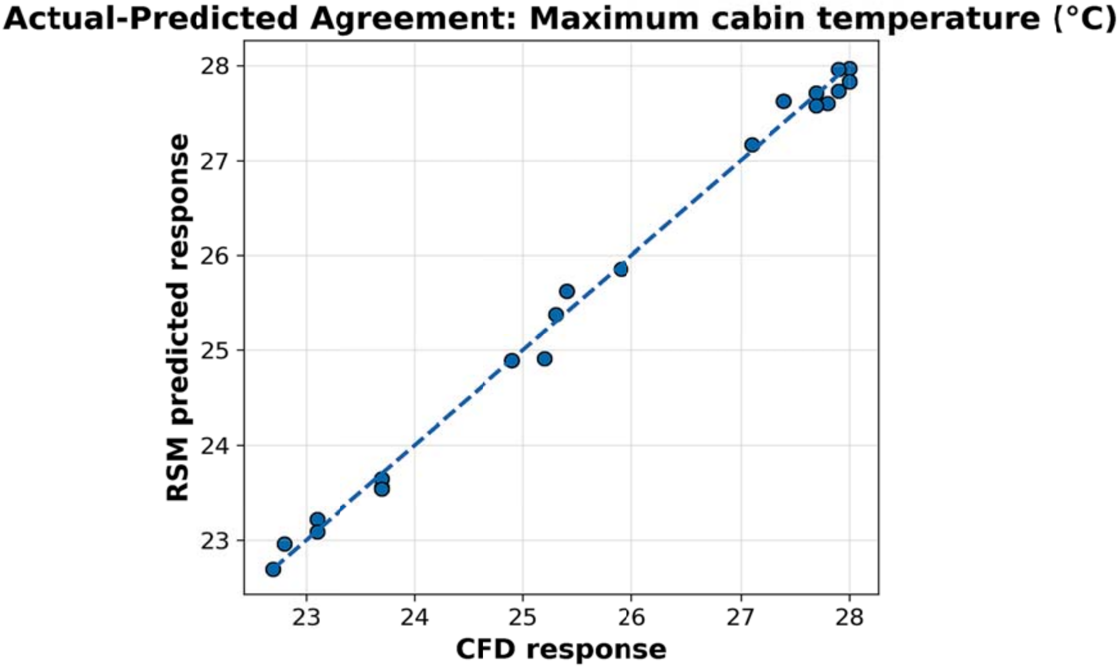

Figure 11. Actual-predicted agreement for the maximum cabin temperature model.

3.4 Response-surface interpretation

The velocity response surface increased as inlet velocity rose. The temperature response surface was more sensitive to inlet temperature than to inlet velocity. These trends show why the ECS setting must be chosen from the combined response, not from one variable alone. High supply velocity can strengthen flushing of weak-flow zones, but it can also increase local draught. Low supply temperature reduces thermal peaks, but local comfort still depends on the velocity field, turbulence level and seat-row location.

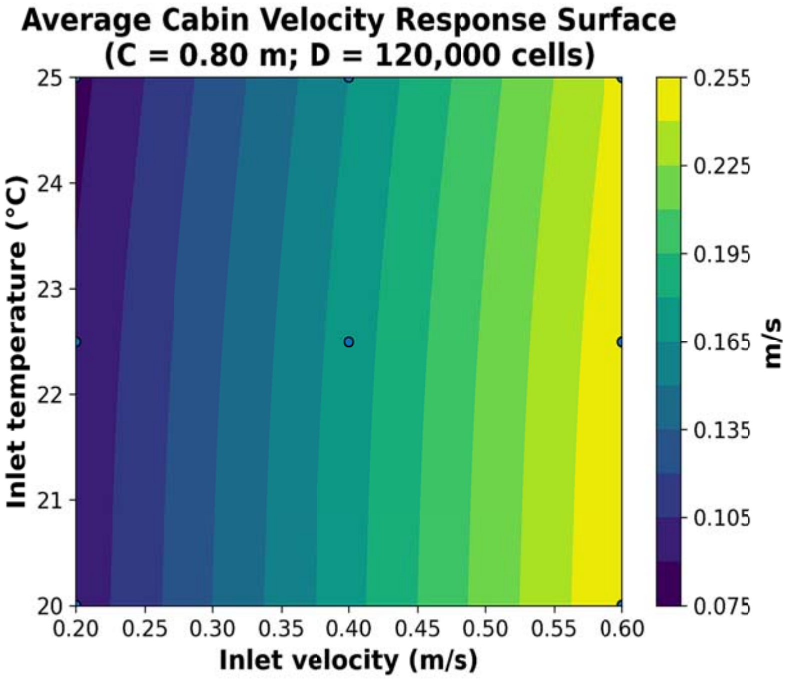

Figure 12. Response surface for average cabin velocity at representative seat pitch and mesh level.

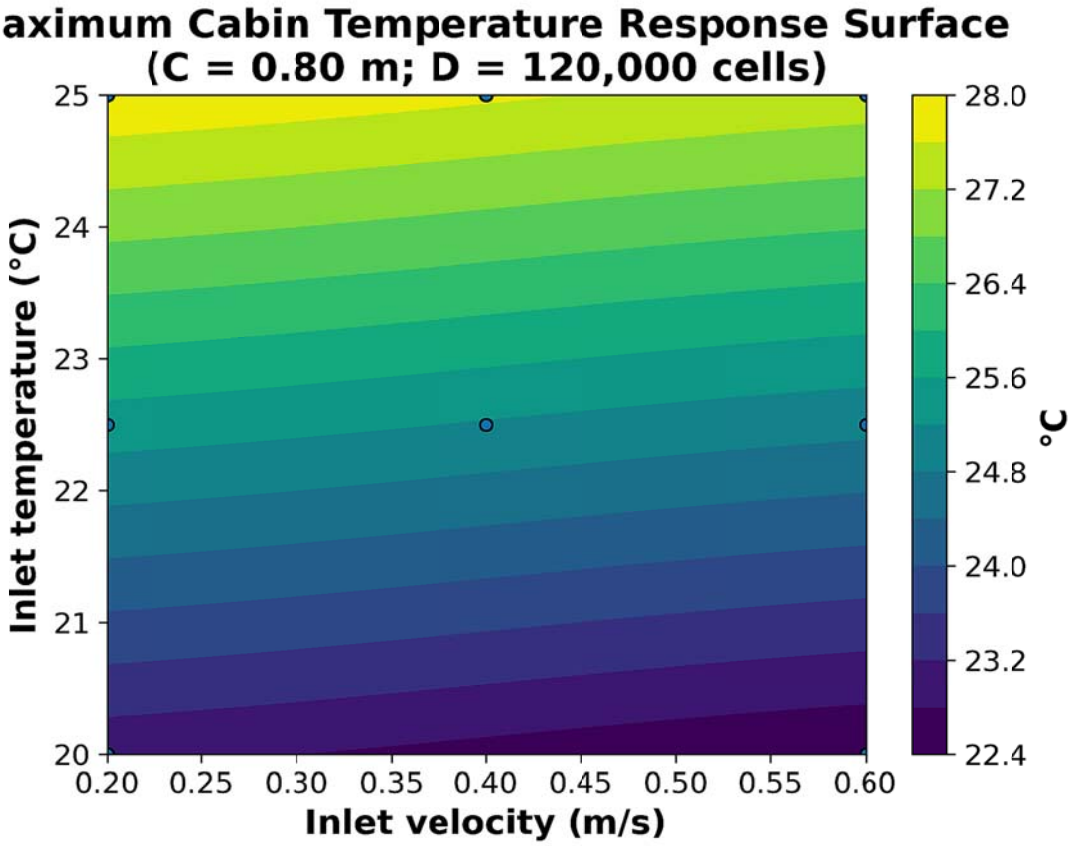

Figure 13. Response surface for maximum cabin temperature at representative seat pitch and mesh level.

3.5 Multi-response desirability optimisation

The desirability solution identified a low-velocity, low-temperature operating point near the lower boundary of the supply settings, combined with the finest mesh level included in the numerical design. The airflow objective was treated as a low-draught bulk-velocity target rather than a maximum-velocity objective. The predicted average velocity of 0.099 m/s is close to the smallest tabulated CFD value of 0.10 m/s because of model interpolation and rounding within the investigated design region. The corresponding predicted maximum temperature of 24.275 °C lies within the simulated thermal range and agrees with the expected effect of lower inlet temperature on thermal peaks.

Table 8. Multi-response desirability solution from the RSM optimisation.

Quantity	Optimised value
Inlet velocity	0.201 m/s
Inlet temperature	20.595 °C
Seat pitch	0.709 m
Mesh refinement	150,000 cells
Predicted average cabin velocity	0.099 m/s
Predicted maximum cabin temperature	24.275 °C
Composite desirability	1.000

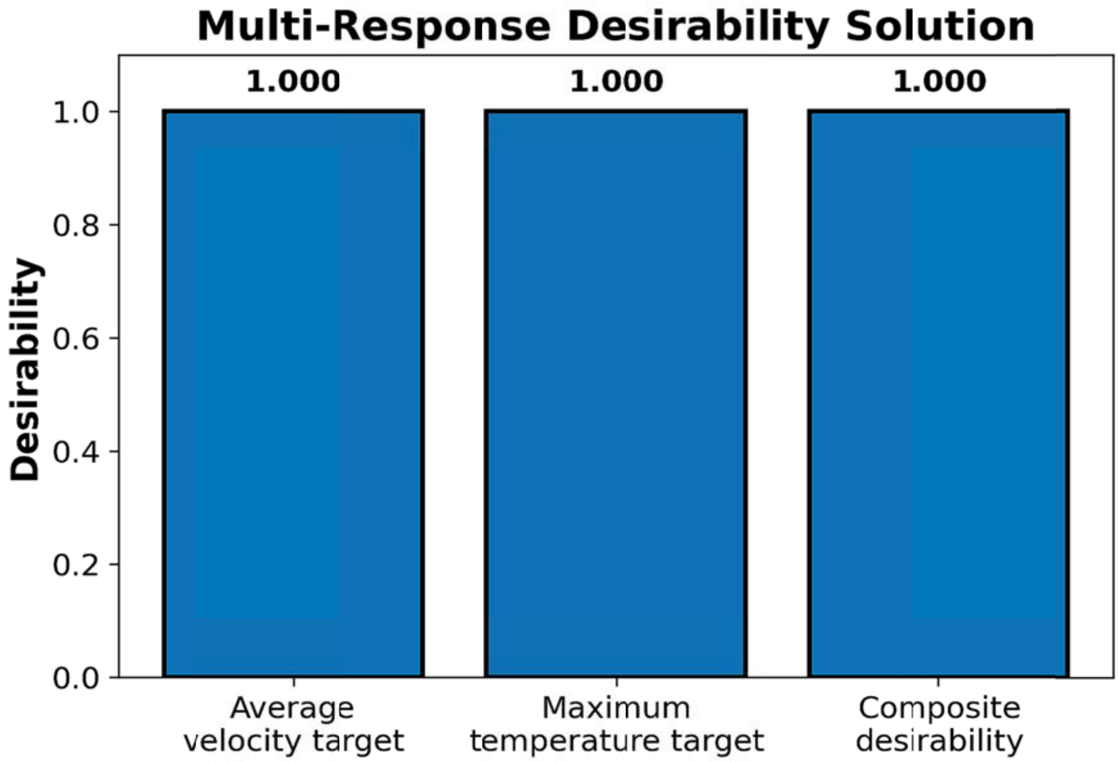

Figure 14. Desirability interpretation for the combined airflow and thermal objectives.

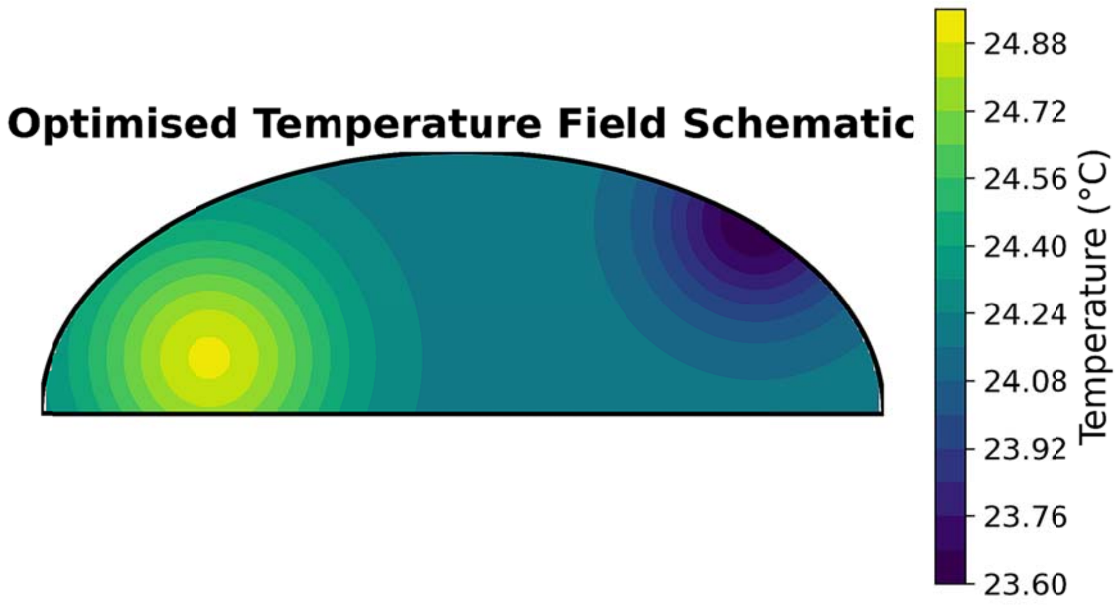

Figure 15. Optimised temperature-field schematic redrawn from the CFD-RSM interpretation at the selected RSM setting.

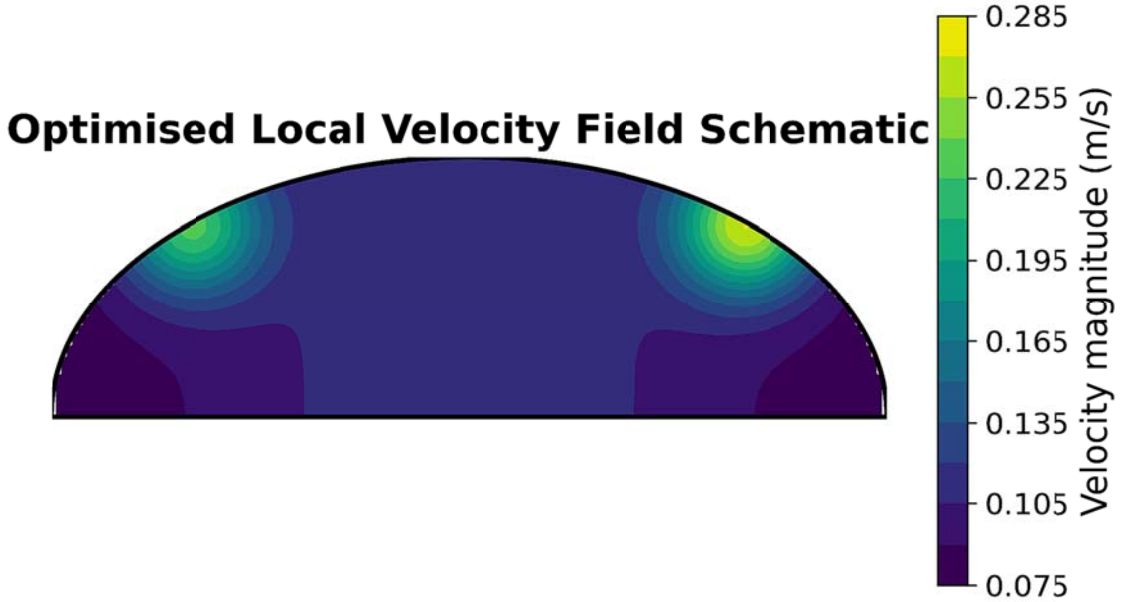

Figure 16. Optimised local-velocity-field schematic redrawn from the CFD-RSM interpretation at the selected RSM setting. The colour scale represents local velocity magnitude, while the response variable is volume-averaged cabin velocity.

4. Discussion

Supply momentum and supply temperature controlled different parts of the cabin response. Inlet velocity dominated the bulk airflow response because it controls the momentum introduced into the cabin section. Raising inlet velocity can strengthen jet penetration and local flushing, but excessive local velocity may cause draught in occupied regions. The velocity response therefore defines the supply-air range that should be examined with local comfort metrics.

Inlet temperature dominated the thermal response because it sets the thermal condition of the entering air. The trend is physically consistent: colder supply air reduces maximum cabin temperature, while warmer supply air increases the probability of thermal peaks. A complete comfort judgement would still require local air temperature, air speed, turbulence intensity, humidity and radiant effects to be evaluated together using recognised comfort metrics [1-3].

Seat pitch affected both responses. Wider row spacing reduces the obstruction imposed by the seat row and changes the passages through which supply jets move after entering the cabin. This explains why seat pitch had a measurable influence even though it is not an ECS operating parameter. The result also shows that cabin-layout choices and ECS settings are linked; a supply condition that performs adequately under one seat-pitch arrangement may not behave the same way under another.

Mesh refinement was retained as a numerical-control factor. Its weak effect on the average-velocity response suggests that the bulk airflow indicator was not strongly mesh-dependent within the tested range. Its stronger effect on maximum temperature indicates that thermal peaks are more sensitive to local resolution, especially near walls, seats and supply jets where gradients are steep.

Average cabin velocity was interpreted as a bulk airflow indicator rather than as a spatial uniformity measure. A fuller ventilation assessment should include velocity standard deviation, coefficient of variation, air diffusion performance index, age of air or low-velocity volume fraction, because these measures describe distribution quality beyond a single average value [16]. The extracted model outputs did not include lack-of-fit, adjusted R^2, predicted R^2 or RMSE values, so model adequacy was judged from the available ANOVA, residual degrees of freedom and actual-predicted agreement. PMV, PPD and draught-rate indicators should also be assessed before the selected supply setting is treated as a comfort-verified cabin solution.

5. Conclusion

The CFD-RSM assessment quantified airflow and thermal performance in an Airbus A320 economy-class cabin section. The 24-case simulation campaign varied inlet velocity, inlet temperature, seat pitch and mesh refinement, and evaluated average cabin velocity and maximum cabin temperature from the same CFD matrix.

Average cabin velocity ranged from 0.10 to 0.27 m/s, while maximum cabin temperature ranged from 22.7 to 28.0 °C. Inlet velocity was the dominant factor for the airflow response, and inlet temperature was the dominant factor for the thermal response. Seat pitch influenced both responses because it altered the blockage and passage geometry around the seat row.

The desirability solution predicted an inlet velocity of 0.201 m/s, inlet temperature of 20.595 °C, seat pitch of 0.709 m and mesh refinement of 150,000 cells. The corresponding predicted responses were 0.099 m/s average cabin velocity and 24.275 °C maximum cabin temperature. The velocity value is effectively at the lower boundary of the simulated response range after model interpolation and rounding. This operating point provides a selected ECS supply setting for verification with local comfort and velocity-distribution metrics.

References

[1] Fanger, P. O. Assessment of man's thermal comfort in practice. British Journal of Industrial Medicine, 30(4), 313-324, 1973. DOI: 10.1136/oem.30.4.313. URL: https://doi.org/10.1136/oem.30.4.313

[2] de Dear, R. J. and Brager, G. S. Thermal comfort in naturally ventilated buildings: Revisions to ASHRAE Standard 55. Energy and Buildings, 34(6), 549-561, 2002. DOI: 10.1016/S0378-7788(02)00005-1. URL: https://doi.org/10.1016/S0378-7788(02)00005-1

[3] Toftum, J. Air movement - good or bad? Indoor Air, 14(s7), 40-45, 2004. DOI: 10.1111/j.1600-0668.2004.00271.x. URL: https://doi.org/10.1111/j.1600-0668.2004.00271.x

[4] Zhang, Z. and Chen, Q. Experimental measurements and numerical simulations of particle transport and distribution in ventilated rooms. Atmospheric Environment, 40(18), 3396-3408, 2006. DOI: 10.1016/j.atmosenv.2006.01.014. URL: https://doi.org/10.1016/j.atmosenv.2006.01.014

[5] Zhang, T., Li, P. and Wang, S. A personal air distribution system with air terminals embedded in chair armrests on commercial airplanes. Building and Environment, 47, 89-99, 2012. DOI: 10.1016/j.buildenv.2011.04.035. URL: https://doi.org/10.1016/j.buildenv.2011.04.035

[6] Liu, W., Mazumdar, S., Zhang, Z., Poussou, S. B., Liu, J., Lin, C. H. and Chen, Q. State-of-the-art methods for studying air distributions in commercial airliner cabins. Building and Environment, 47, 5-12, 2012. DOI: 10.1016/j.buildenv.2011.07.005. URL: https://doi.org/10.1016/j.buildenv.2011.07.005

[7] You, R., Chen, J., Lin, C. H., Wei, D. and Chen, Q. Investigating the impact of gaspers on cabin air quality in commercial airliners with a hybrid turbulence model. Building and Environment, 111, 110-122, 2017. DOI: 10.1016/j.buildenv.2016.10.018. URL: https://doi.org/10.1016/j.buildenv.2016.10.018

[8] Cao, Q., Liu, M., Li, X., Lin, C. H., Wei, D., Ji, S., Zhang, T. and Chen, Q. Influencing factors in the simulation of airflow and particle transportation in aircraft cabins by CFD. Building and Environment, 207, Article 108413, 2022. DOI: 10.1016/j.buildenv.2021.108413. URL: https://doi.org/10.1016/j.buildenv.2021.108413

[9] Nielsen, P. V. Fifty years of CFD for room air distribution. Building and Environment, 91, 78-90, 2015. DOI: 10.1016/j.buildenv.2015.02.035. URL: https://doi.org/10.1016/j.buildenv.2015.02.035

[10] Chen, Q. Ventilation performance prediction for buildings: A method overview and recent applications. Building and Environment, 44(4), 848-858, 2009. DOI: 10.1016/j.buildenv.2008.05.025. URL: https://doi.org/10.1016/j.buildenv.2008.05.025

[11] Box, G. E. P. and Wilson, K. B. On the experimental attainment of optimum conditions. Journal of the Royal Statistical Society: Series B, 13(1), 1-45, 1951. DOI: 10.1111/j.2517-6161.1951.tb00067.x. URL: https://doi.org/10.1111/j.2517-6161.1951.tb00067.x

[12] Box, G. E. P. and Behnken, D. W. Some new three level designs for the study of quantitative variables. Technometrics, 2(4), 455-475, 1960. DOI: 10.1080/00401706.1960.10489912. URL: https://doi.org/10.1080/00401706.1960.10489912

[13] Derringer, G. and Suich, R. Simultaneous optimization of several response variables. Journal of Quality Technology, 12(4), 214-219, 1980. DOI: 10.1080/00224065.1980.11980968. URL: https://doi.org/10.1080/00224065.1980.11980968

[14] Shih, T. H., Liou, W. W., Shabbir, A., Yang, Z. and Zhu, J. A new k-epsilon eddy-viscosity model for high-Reynolds-number turbulent flows - model development and validation. Computers & Fluids, 24(3), 227-238, 1995. DOI: 10.1016/0045-7930(94)00032-T. URL: https://doi.org/10.1016/0045-7930(94)00032-T

[15] Launder, B. E. and Spalding, D. B. The numerical computation of turbulent flows. Computer Methods in Applied Mechanics and Engineering, 3(2), 269-289, 1974. DOI: 10.1016/0045-7825(74)90029-2. URL: https://doi.org/10.1016/0045-7825(74)90029-2

[16] Zhai, Z. J., Zhang, Z., Zhang, W. and Chen, Q. Y. Evaluation of various turbulence models in predicting airflow and turbulence in enclosed environments by CFD: Part 1 - summary of prevalent turbulence models. HVAC&R Research, 13(6), 853-870, 2007. DOI: 10.1080/10789669.2007.10391459. URL: https://doi.org/10.1080/10789669.2007.10391459

[17] Zhang, Z., Zhang, W., Zhai, Z. J. and Chen, Q. Y. Evaluation of various turbulence models in predicting airflow and turbulence in enclosed environments by CFD: Part 2 - comparison with experimental data from literature. HVAC&R Research, 13(6), 871-886, 2007. DOI: 10.1080/10789669.2007.10391460. URL: https://doi.org/10.1080/10789669.2007.10391460

[18] Wang, M., Lin, C. H. and Chen, Q. Advanced turbulence models for predicting particle transport in enclosed environments. Building and Environment, 47, 40-49, 2012. DOI: 10.1016/j.buildenv.2011.05.018. URL: https://doi.org/10.1016/j.buildenv.2011.05.018

[19] Zhang, T. and Chen, Q. Novel air distribution systems for commercial aircraft cabins. Building and Environment, 42(4), 1675-1684, 2007. DOI: 10.1016/j.buildenv.2006.02.014. URL: https://doi.org/10.1016/j.buildenv.2006.02.014

[20] Gao, N. P. and Niu, J. L. Personalized ventilation for commercial aircraft cabins. Journal of Aircraft, 45(2), 508-512, 2008. DOI: 10.2514/1.30272. URL: https://doi.org/10.2514/1.30272

[21] Zhang, T., Li, P., Zhao, Y. and Wang, S. Various air distribution modes on commercial airplanes. Part 1: Experimental measurement. HVAC&R Research, 19(3), 268-282, 2013. DOI: 10.1080/10789669.2013.765241. URL: https://doi.org/10.1080/10789669.2013.765241

[22] Zhang, T., Li, P., Zhao, Y. and Wang, S. Various air distribution modes on commercial airplanes - Part 2: Computational fluid dynamics modeling and validation. HVAC&R Research, 19(5), 457-470, 2013. DOI: 10.1080/10789669.2013.789368. URL: https://doi.org/10.1080/10789669.2013.789368

[23] Li, B., Duan, R., Li, J., Huang, Y., Yin, H., Lin, C. H., Wei, D., Shen, X., Liu, J. and Chen, Q. Experimental studies of thermal environment and contaminant transport in a commercial aircraft cabin with gaspers on. Indoor Air, 26(5), 806-819, 2016. DOI: 10.1111/ina.12265. URL: https://doi.org/10.1111/ina.12265

[24] Li, J., Cao, X., Liu, J., Shen, X., Lin, C. H. and Chen, Q. PIV experimental research on gasper jets interacting with the main ventilation in an aircraft cabin. Building and Environment, 138, 149-159, 2018. DOI: 10.1016/j.buildenv.2018.04.023. URL: https://doi.org/10.1016/j.buildenv.2018.04.023

[25] Maier, J., Marggraf-Micheel, C., Dehne, T., Bosbach, J. and Lange, P. Thermal comfort of different displacement ventilation systems in an aircraft passenger cabin. Building and Environment, 111, 256-264, 2017. DOI: 10.1016/j.buildenv.2016.11.017. URL: https://doi.org/10.1016/j.buildenv.2016.11.017

[26] Maier, J., Marggraf-Micheel, C., Dehne, T. and Bosbach, J. Ceiling-based cabin displacement ventilation in an aircraft passenger cabin: Analysis of thermal comfort. Building and Environment, 146, 29-39, 2018. DOI: 10.1016/j.buildenv.2018.09.031. URL: https://doi.org/10.1016/j.buildenv.2018.09.031

[27] Liu, M., Chang, D., Liu, J., Ji, S., Lin, C. H., Wei, D., Long, Z., Zhang, T., Shen, X., Cao, Q., Li, X., Zeng, X. and Li, H. Experimental investigation of air distribution in an airliner cabin mockup with displacement ventilation. Building and Environment, 191, Article 107577, 2021. DOI: 10.1016/j.buildenv.2020.107577. URL: https://doi.org/10.1016/j.buildenv.2020.107577

[28] Zhang, T., Lin, C. H. and Chen, Q. Performance evaluation of different air distribution systems in an aircraft cabin mockup. Aerospace Science and Technology, 70, 359-366, 2017. DOI: 10.1016/j.ast.2017.08.009. URL: https://doi.org/10.1016/j.ast.2017.08.009

[29] Zhang, Z. and Chen, Q. Comparison of the Eulerian and Lagrangian methods for predicting particle transport in enclosed spaces. Atmospheric Environment, 41(25), 5236-5248, 2007. DOI: 10.1016/j.atmosenv.2006.05.086. URL: https://doi.org/10.1016/j.atmosenv.2006.05.086

[30] Li, Y. and Nielsen, P. V. CFD and ventilation research. Indoor Air, 21(6), 442-453, 2011. DOI: 10.1111/j.1600-0668.2011.00723.x. URL: https://doi.org/10.1111/j.1600-0668.2011.00723.x

[31] Posner, J. D., Buchanan, C. R. and Dunn-Rankin, D. Measurement and prediction of indoor air flow in a model room. Energy and Buildings, 35(5), 515-526, 2003. DOI: 10.1016/S0378-7788(02)00163-9. URL: https://doi.org/10.1016/S0378-7788(02)00163-9